Schweizerischer Erdbebendienst
Service Sismologique Suisse
Servizio Sismico Svizzero
Servizi da Terratrembels Svizzer

Eidgenössische Technische Hochschule Zürich
Swiss Federal Institute of Technology Zurich

Aigle - rue de la Gare (SAIG)

SITE CHARACTERIZATION REPORT

Clotaire MICHEL, Carlo CAUZZI, Daniel ROTEN,

Jan BURJANEK, Valerio POGGI, Donat FÄH

Sonneggstrasse 5 CH-8092 Zürich Switzerland; E-mail: clotaire.michel@sed.ethz.ch

Last modified : November 5, 2013

Abstract

Ambient vibration array measurements were performed to characterize the alluvial fan in Aigle, close to the train station. The site, where the new station SAIG of the Swiss Strong Motion Network was installed, is located close to the old city centre where heavy damage was reported in 1564. In order to characterize the velocity profile under the station, array measurements with a $200\,\mathrm{m}$ aperture were performed. The measurements were successful and allowed deriving a velocity model for this site. The soil column underlying station SAIG is first the alluvial fan of the "Cône de la Grande Eau" made of gravels approximately in the first $50\,\mathrm{m}$ divided in 2 layers of with an interface at about $15\,\mathrm{m}$ and velocities of 500 and $700\,\mathrm{m/s}$, respectively. Below, the consolidated sediments of the Rhone ($1500\,\mathrm{m/s}$) can be considered as rock. The bedrock is found at $350\,\mathrm{m}$ depth. The fundamental resonance frequency is $1.4\,\mathrm{Hz}$ with a polarized motion in the direction of the alluvial fan, therefore possibly corresponding to a 2D/3D behaviour of this structure. $V_{s,30}$ is found equal to $535\,\mathrm{m/s}$, corresponding to ground type B for EC8 [CEN, 2004] and SIA261 [SIA, 2003]. The theoretical SH transfer function and impedance contrast of the quarter-wavelength velocity computed from the inverted profiles show an amplification up to 4 at $3\,\mathrm{Hz}$, corresponding to the resonance of the "Cône de la Grande Eau" gravels. Recordings of the new station will allow to validate these simple models.

Contents

1 Introduction

The station SAIG (Aigle - rue de la Gare) is part of the Swiss Strong Motion Network (SSMNet) in the Rhone valley. SAIG has been installed in the framework of the SSMNet Renewal project in 2012. This project includes also the site characterization. The passive array measurements have been selected as a standard tool to investigate these sites. The measurement campaign was carried out on 27th June 2012 in the park "Mon Séjour" and around (Fig. 1), with a centre close to station SAIG, in order to characterize the sediments under this station. The historical city of Aigle suffered heavy damage in 1564 due to a $M \approx 6$ earthquake. According to the geological map, this station is located on a large alluvial fan ("Cône de la Grande Eau") superimposing the Rhone sediments. This report presents the measurement setup, the results of the H/V analysis and of the array processing of the surface waves (dispersion curves). Then, an inversion of these results into velocity profiles is performed and interpreted with the help of existing boreholes. Standard parameters are derived to evaluate the amplification at this site.

Canton	City	Location	Station code	Site type	Slope
Vaud	Aigle	Mon Séjour	SAIG	Alluvial fan	Flat

Table 1: Main characteristics of the study-site.

Figure 1: Picture of the site.

2 Experiment description

2.1 Ambient Vibrations

The ground surface is permanently subjected to ambient vibrations due to:

- natural sources (ocean and large-scale atmospheric phenomena) below $1\,\mathrm{Hz}$,
- local meteorological conditions (wind and rain) at frequencies around $1\,\mathrm{Hz}$,
- human activities (industrial machines, traffic…) at frequencies above $1\,\mathrm{Hz}$ [Bonnefoy-Claudet et al., 2006].

The objective of the measurements is to record these ambient vibrations and to use their propagation properties to infer the underground structure. First, the polarization of the recorded waves (H/V ratio) is used to derive the resonance frequencies of the soil column. Second, the arrival time delays at many different stations are used to derive the velocity of surface waves at different frequencies (dispersion). The information (H/V, dispersion curves) is then used to derive the properties of the soil column using an inversion process.

2.2 Equipment

For these measurements 12 Quanterra Q330 dataloggers named NR01 to NR12 and 14 Lennartz 3C 5 s seismometers were available (see Tab. 2). Each datalogger can record on 2 ports A (channels EH1, EH2, EH3 for Z, N, E directions) and B (channels EH4, EH5, EH6 for Z, N, E directions). Time synchronization was ensured by GPS. The sensors were placed on a metal tripod in a $20\,\mathrm{cm}$ deep hole, when possible, for better coupling with the ground.

Digitizer	**Model**	**Number**	**Resolution**
	Quanterra Q330	12	$24\,\mathrm{bits}$
Sensor type	**Model**	**Number**	**Cut-off frequency**
Velocimeter	Lennartz 3C	14	$0.2\,\mathrm{Hz}$

Table 2: Equipment used.

2.3 Geometry of the arrays

Two array configurations were used, for a total of 4 rings of 10, 25, 50 and $100\,\mathrm{m}$ radius around a central station. The first configuration includes the 3 inner rings with 14 sensors; the second configuration includes the 2 outer rings (plus the first ring) with 14 sensors. The minimum inter-station distance and the aperture are therefore 10 and $100\,\mathrm{m}$ and 10 and $200\,\mathrm{m}$, respectively. The experimental setup is displayed in Fig. 2. The final usable datasets are detailed in section 3.2.

Figure 2: Geometry of the arrays.

2.4 Positioning of the stations

The sensor coordinates were measured using a differential GPS device (Leica Viva GS10), including only a rover station and using the Real Time Kinematic technique provided by Swisstopo. However, the GSM module did not work (wrong configuration) and only GPS raw data was written during 5 min at each point, without control on the precision. Post-processing was performed using the Leica-Geo Office software and a Virtual Reference provided by Swisstopo. It allowed an absolute positioning with an accuracy better than $5\,\mathrm{cm}$ on the Swissgrid except for point AIG402 with a precision of $15\,\mathrm{cm}$ and point AIG401 with $7.5\,\mathrm{cm}$. This precision was assumed sufficient for this processing.

3 Data quality

3.1 Usable data

The largest time windows were extracted, for which all the sensors of the array were correctly placed and the GPS synchronization was ensured. For the first dataset, point AIG305 is advised not to be used because it was kicked by a worker and re-positioned at 9:40. The array was limited in size by main roads and train lines, where the traffic was not negligible. The temperature was high but it does not seem it affected the recordings. GPS measurement, relatively long, were performed during the recordings.

The spectra show that point AIG202 has abnormal amplitudes below $2\,\mathrm{Hz}$ in the vertical direction. Point AIG401 shows abnormally high amplitudes in all direction, possibly due to the proximity to the train line. Its removal for the processing could be considered, even though it was used in the following. Point AIG405 was also noisy due to the road but it does not seem critical. Point AIG301 shows a strange peak in the vertical direction around $0.9\,\mathrm{Hz}$.

The characteristics of the datasets are detailed in Tab. 3.

3.2 Data processing

The data were first converted to SAC format including in the header the coordinates of the point (CH1903 system), the recording component and a name related to the position. The name is made of 3 letters characterizing the location (AIG here), 1 digit for the ring and 2 more digits for the number in the ring. Recordings were not corrected for instrumental response.

Dataset	Starting Date	Time	Length	F_s	Min. inter-distance	Aperture	# of points
1	2012/06/27	8:32	117 min	200 Hz	10 m	100 m	14
2	2012/06/27	11:10	123 min	200 Hz	10 m	200 m	14

Table 3: Usable datasets.

4 H/V processing

4.1 Processing method and parameters

In order to process the H/V spectral ratios, several codes and methods were used. The classical H/V method was applied using the Geopsy `http://www.geopsy.org` software. In this method, the ratio of the smoothed Fourier Transform of selected time windows are averaged. Tukey windows (cosine taper of 5% width) of $50\,\mathrm{s}$ long overlapping by 50% were selected. Konno and Ohmachi [1998] smoothing procedure was used with a b value of 80. The classical method computed using the method of Fäh et al. [2001] was also performed.

Moreover, the time-frequency analysis method [Fäh et al., 2009] was used to estimate the ellipticity function more accurately using the Matlab code of V. Poggi, available in the software repository of the engineering seismology group of SED. In this method, the time-frequency analysis using the Wavelet transform is computed for each component. For each frequency, the maxima over time (10 per minute with at least $0.1\,\mathrm{s}$ between each) in the TFA are determined. The Horizontal to Vertical ratio of amplitudes for each maximum is then computed and statistical properties for each frequency are derived. A Cosine wavelet with parameter 9 is used. The mean of the distribution for each frequency is stored. For the sake of comparison, the time-frequency analysis of Fäh et al. [2001], based on the spectrogram, was also used, as well as the wavelet-based TFA coded in Geopsy.

The ellipticity extraction using the Capon analysis [Poggi and Fäh, 2010] (see section on array analysis) were also performed.

Method	Freq. band	Win. length	Anti-trig.	Overlap	Smoothing
Standard H/V Geopsy	$0.2 - 20\,\mathrm{Hz}$	$50\,\mathrm{s}$	No	50%	K&O 80
Standard H/V D. Fäh	$0.2 - 20\,\mathrm{Hz}$	$30\,\mathrm{s}$	No	75%	-
H/V TFA Geopsy	$0.2 - 20\,\mathrm{Hz}$	Morlet m=8 fi=1	No	-	-
H/V TFA D. Fäh	$0.2 - 20\,\mathrm{Hz}$	Specgram	No	-	-
H/V TFA V. Poggi	$0.2 - 20\,\mathrm{Hz}$	Cosine wpar=9	No	-	No

Table 4: Methods and parameters used for the H/V processing.

4.2 Results

Considering the quality of the recordings, point AIG202 was removed. As remarked in the section on the data quality, a peak at $0.9\,\mathrm{Hz}$ is affecting the results for point AIG301, but its behaviour at higher frequency is still comparable to the other points. Except these issues, other H/V curves are consistently showing a peak at $1.3 - 1.4\,\mathrm{Hz}$ (Fig. 3). The external ring shows slightly different curves compared to the other points but the peak values are not significantly different.

Moreover, all the methods to compute H/V ratios are compared at the array centre on Fig. 4, in which the classical methods were divided by $\sqrt{2}$ to correct from the Love wave contribution [Fäh et al., 2001]. The classical and TFA methods match well but the peak value is slightly

different for each method. The 3C FK analysis (Capon method) does not have resolution down to the peak but matches also perfectly above 2 Hz.

Looking at the H/V values available in the city-centre of Aigle (Fig. 5), the gradient from the array (1.35 Hz) to the old city-centre (1.5 Hz) is low and station SAIG can be considered as representative for the whole city-centre. It should be noticed that other H/V data is available in the city of Aigle in the SED database but the recordings were found to be of too low quality to be used.

The peak at the SAIG station is therefore at 1.4 Hz, with a peak amplitude around 4 for the TFA methods.

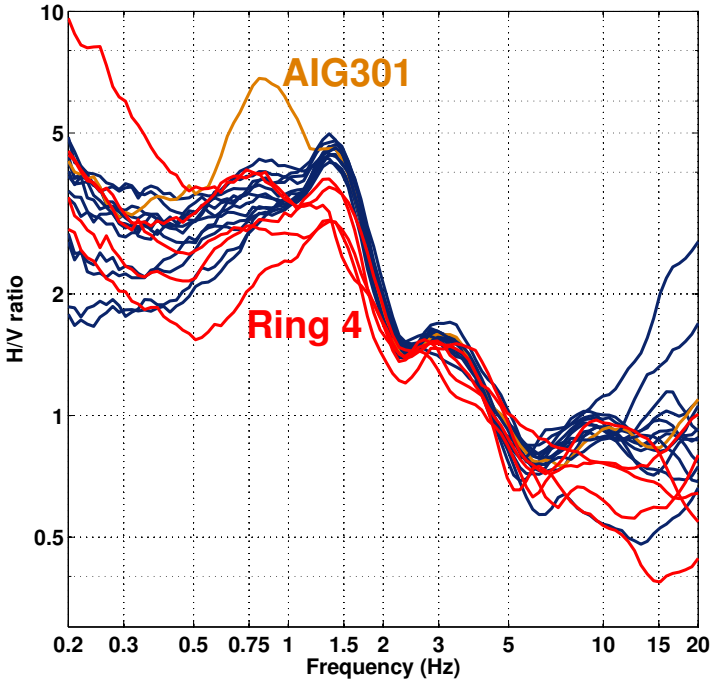

Figure 3: H/V spectral ratios (time-frequency analysis code V. Poggi).

4.3 Polarization analysis

A polarization analysis using the code of Burjánek et al. [2010] was performed in order to determine if the observed H/V peak is related to an eventual 2D resonance. The results show the motion is horizontally polarized at the resonance frequency (H/V peak) with a relatively clear preferred polarization in the ENE-WSW direction, i.e. in the direction of the alluvial fan (Fig. 6). This result is consistent throughout the array. This resonance may therefore correspond to a 2D/3D resonance of the alluvial fan "Cône de la Grande Eau". The effect is not very strong, but it should be kept in mind for future analyses.

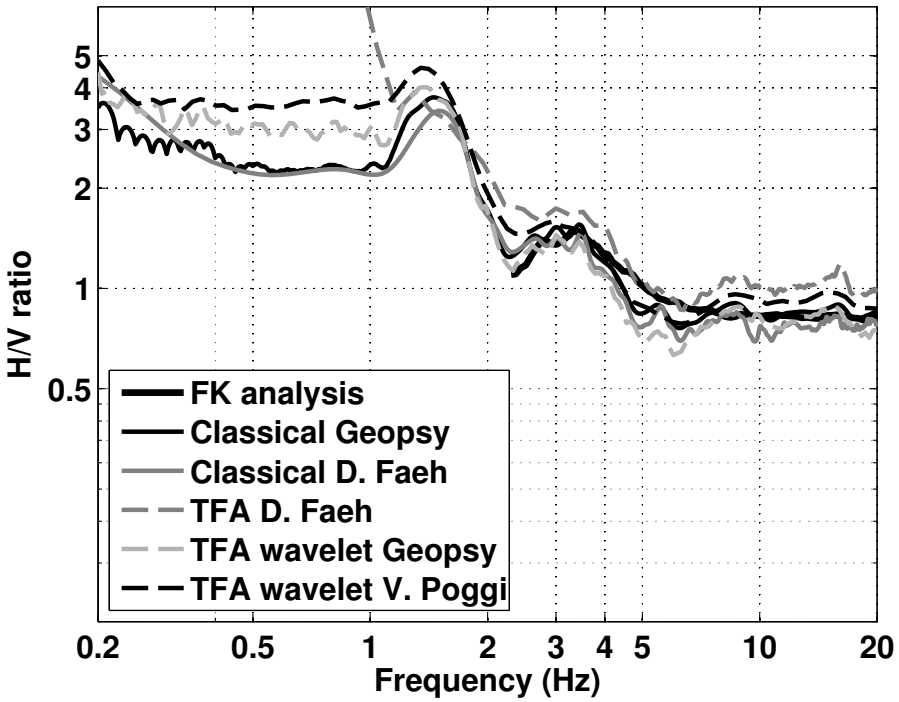

Figure 4: H/V spectral ratios for point AIG000 using the different codes. Classical methods were divided by $\sqrt{2}$.

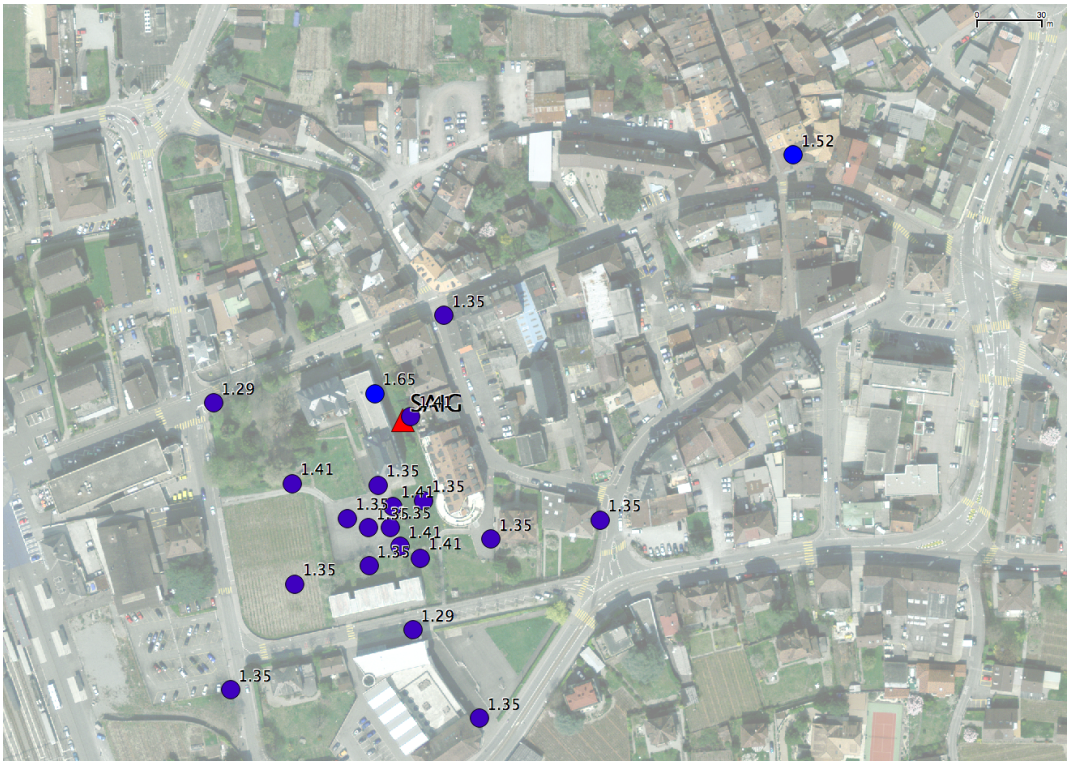

Figure 5: Map of the H/V resonance frequency in the city-centre of Aigle.

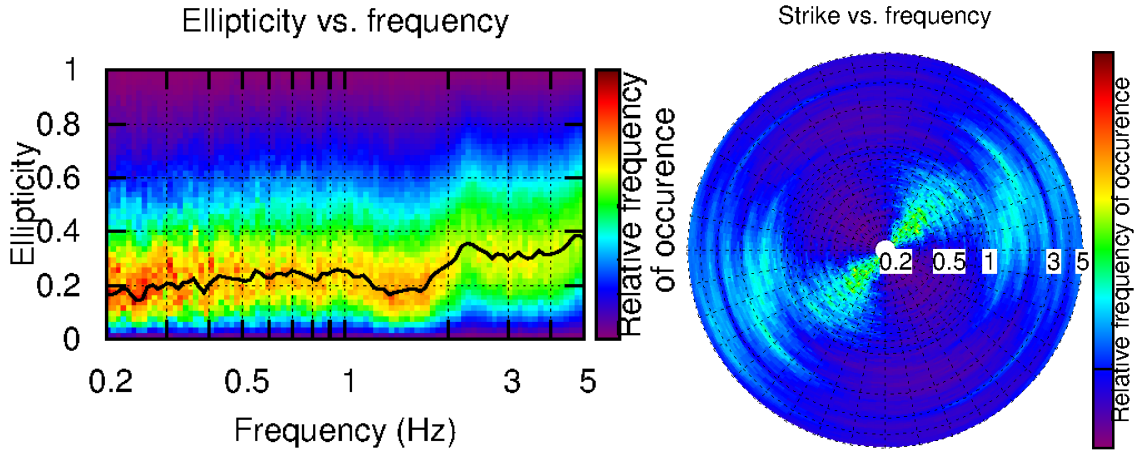

Figure 6: Polarization analysis at point AIG000. Left: Ellipticity (A trough in the ellipticity corresponds to horizontally polarized motion). Right: Strike of the polarization.

5 Array processing

5.1 Processing methods and parameters

The vertical components of the arrays were processed using the FK and the High-resolution FK analysis [Capon, 1969] using the Geopsy `http://www.geopsy.org` software. Better results were obtained using large time windows (300T). The results of computations of both datasets were merged to estimate the dispersion curves.

Moreover, a 3C array analysis [Fäh et al., 2008] was also performed using the array_tool_3C software [Poggi and Fäh, 2010]. It allows to derive Rayleigh and Love modes including the Rayleigh ellipticity. The results of computations of both datasets were merged to estimate the dispersion curves.

Method	Set	Freq. band	Win. length	Anti-trig.	Overlap	Grid step	Grid size	# max.
HRFK 1C	1	$1.5 - 30\,\mathrm{Hz}$	$300T$	No	50%	0.001	0.6	5
HRFK 1C	2	$1.5 - 30\,\mathrm{Hz}$	$300T$	No	50%	0.001	0.6	5
HRFK 3C	1	$1.5 - 30\,\mathrm{Hz}$	Wav. 10 Tap. 0.2	No	50%	200 m/s	3000 m/s	5
HRFK 3C	2	$1.5 - 30\,\mathrm{Hz}$	Wav. 10 Tap. 0.2	No	50%	200 m/s	3000 m/s	5

Table 5: Methods and parameters used for the array processing.

5.2 Obtained dispersion curves

The first Rayleigh mode in the 1C FK analysis could be picked between 2.5 and $25\,\mathrm{Hz}$ (Fig. 7) including its standard deviation. The velocities are ranging from $1500\,\mathrm{m/s}$ at $2.5\,\mathrm{Hz}$ down to $400\,\mathrm{m/s}$ at $25\,\mathrm{Hz}$. Moreover, what could be the first higher mode can be seen on the second dataset and was picked as well.

Using the 3C analysis, both fundamental Rayleigh and Love modes can be picked (Fig. 7). The radial component also provides the Rayleigh fundamental mode. The fundamental Rayleigh mode shows no difference with the 1C analysis (Fig. 8), although it is more securely picked at low frequency thanks to the log scale. Rayleigh fundamental mode is picked from 3.1 to $25\,\mathrm{Hz}$ and Love from 2.4 to $24\,\mathrm{Hz}$ (Fig. 8). Moreover, the first Love higher mode was also picked from the second dataset. It happens to be similar to the first Rayleigh mode.

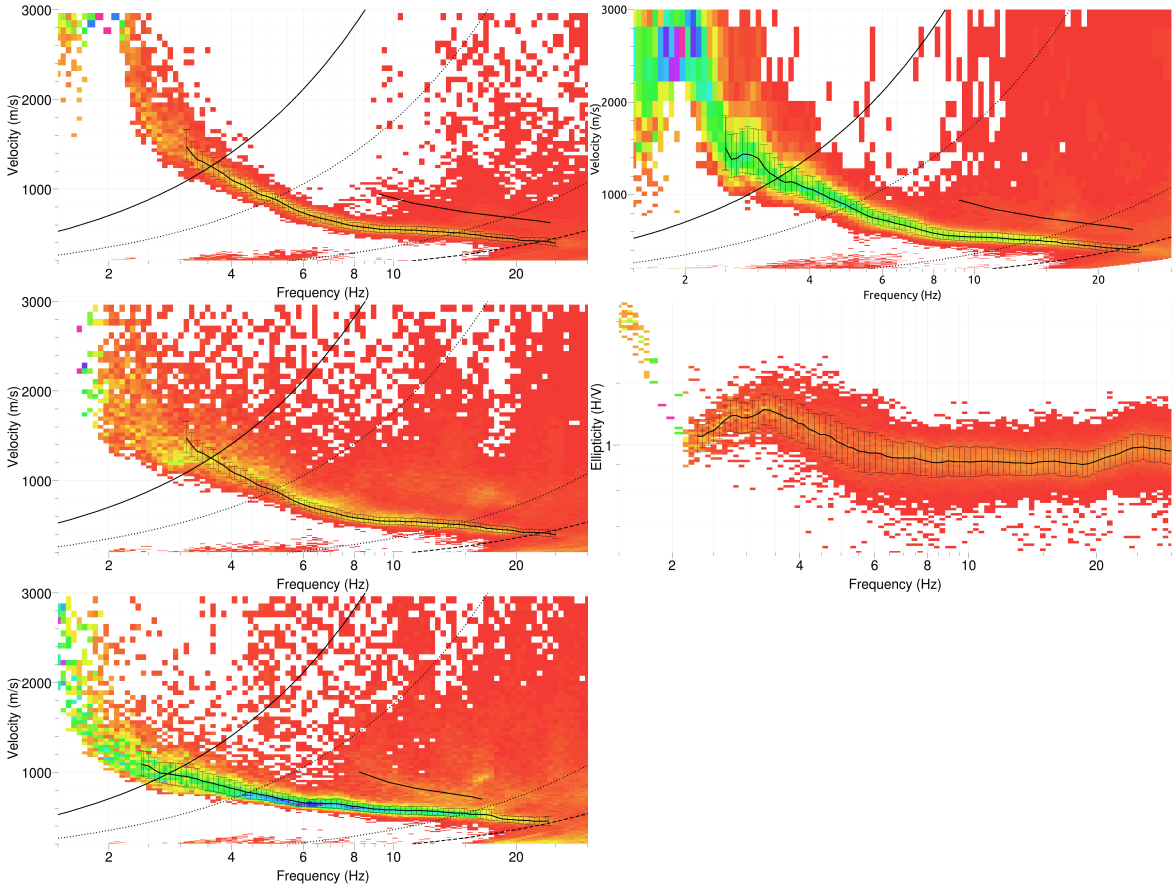

Figure 7: Dispersion curves obtained from the 3C (left) and 1C (top right) array analysis (top: vertical; centre: radial; bottom: transverse components) and ellipticity from 3C analysis (centre right).

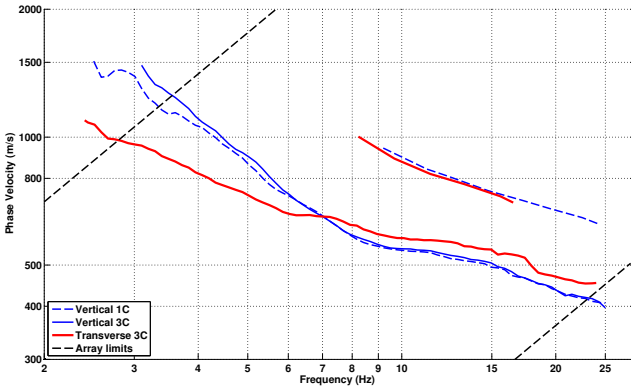

Figure 8: Picked dispersion curves from 1C and 3C FK methods.

6 Inversion and interpretation

6.1 Inversion

For the inversion, Rayleigh and Love fundamental and first higher modes dispersion curves (3C analysis), as well as the right flank of the ellipticity and the ellipticity peak (TFA analysis) were used as simultaneous targets, without standard deviation to avoid different weighting. A weight of 0.3 was assigned to the ellipticity curves. All curves were resampled using 50 points between 1 and $25\,\mathrm{Hz}$ in log scale.

The inversion was performed using the Improved Neighborhood Algorithm (NA) Wathelet [2008] implemented in the Dinver software. In this algorithm, the tuning parameters are the following: Ns_0 is the number of starting models, randomly distributed in the parameter space, Nr is the the number of best cells considered around these Ns_0 models, Ns is the number of new cells generated in the neighborhood of the Nr cells (Ns/Nr per cell) and It_{max} is the number of iteration of this process. The process ends with $Ns_0 + Nr * \frac{Ns}{Nr} * It_{max}$ models. The used parameters are detailed in Tab. 6.

It_{max}	Ns_0	Ns	Nr
500	10000	100	100

Table 6: Tuning parameters of Neighborhood Algorithm.

During the inversion process, low velocity zones were not allowed. The Poisson ratio was inverted in each layer in the range 0.2-0.4, up to 0.47 below the assumed water table. The density was supposed equal to $2000\,\mathrm{kg/m^3}$ except for the layers assumed to be rock ($2500\,\mathrm{kg/m^3}$). Inversions with free layer depths as well as fixed layer depths were performed. 4 layers are enough to explain most of the targets (dispersion and ellipticity), but more layers are used to smooth the obtained results and better explore the parameter space. 5 independent runs of 5 different parametrization schemes (5 and 7 layers over a half space and 10, 12 and 14 layers with fixed depth) were performed. For further elaborations, the best models of these 25 runs were selected (Fig. 12).

The inversion leads to a first layer of $12 - 15\,\mathrm{m}$ already at a velocity of about $500\,\mathrm{m/s}$. Below, a clear layer down to about $45 - 60\,\mathrm{m}$ has a velocity of $700\,\mathrm{m/s}$. Below this interface, the velocity increases with a gradient shape to about $1500\,\mathrm{m/s}$ down to the "bedrock", located between 300 and $350\,\mathrm{m}$. The velocity in the bedrock is found to be around $3000\,\mathrm{m/s}$ but is actually not well constrained. When comparing to the target curves (Fig. 10 and Fig. 11), all curves, imposing a heavy constraint, are well represented. The two first layer, down to $45-60\,\mathrm{m}$, are generating a resonance around $3\,\mathrm{Hz}$, whereas the bedrock is creating the fundamental peak at $1.4\,\mathrm{Hz}$.

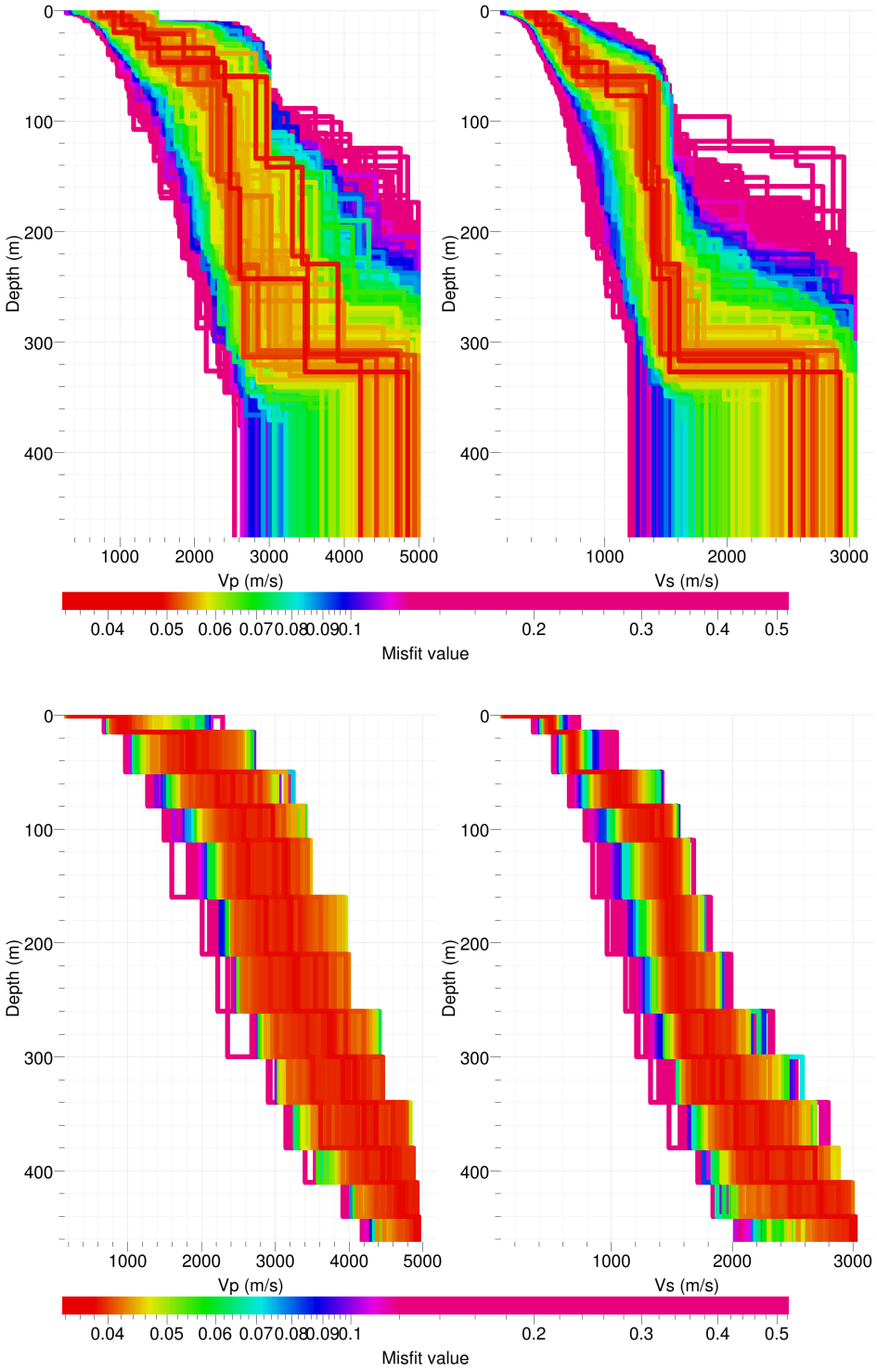

Figure 9: Inverted ground profiles in terms of V_p and V_s; top: free layer depth strategy; bottom: fixed layer depth strategy.

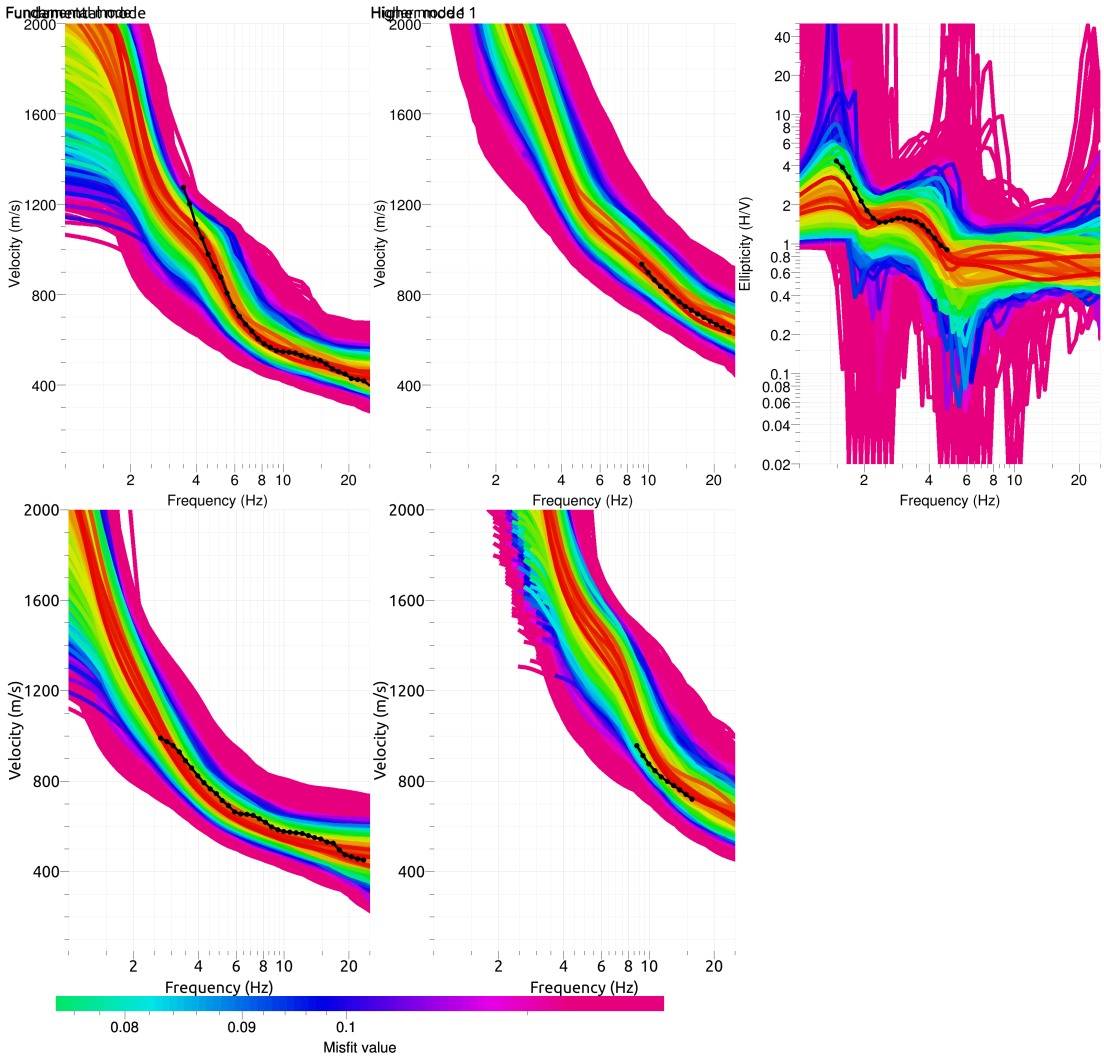

Figure 10: Comparison between inverted models and measured Rayleigh and Love modes and corresponding ellipticity, free layer depth strategy.

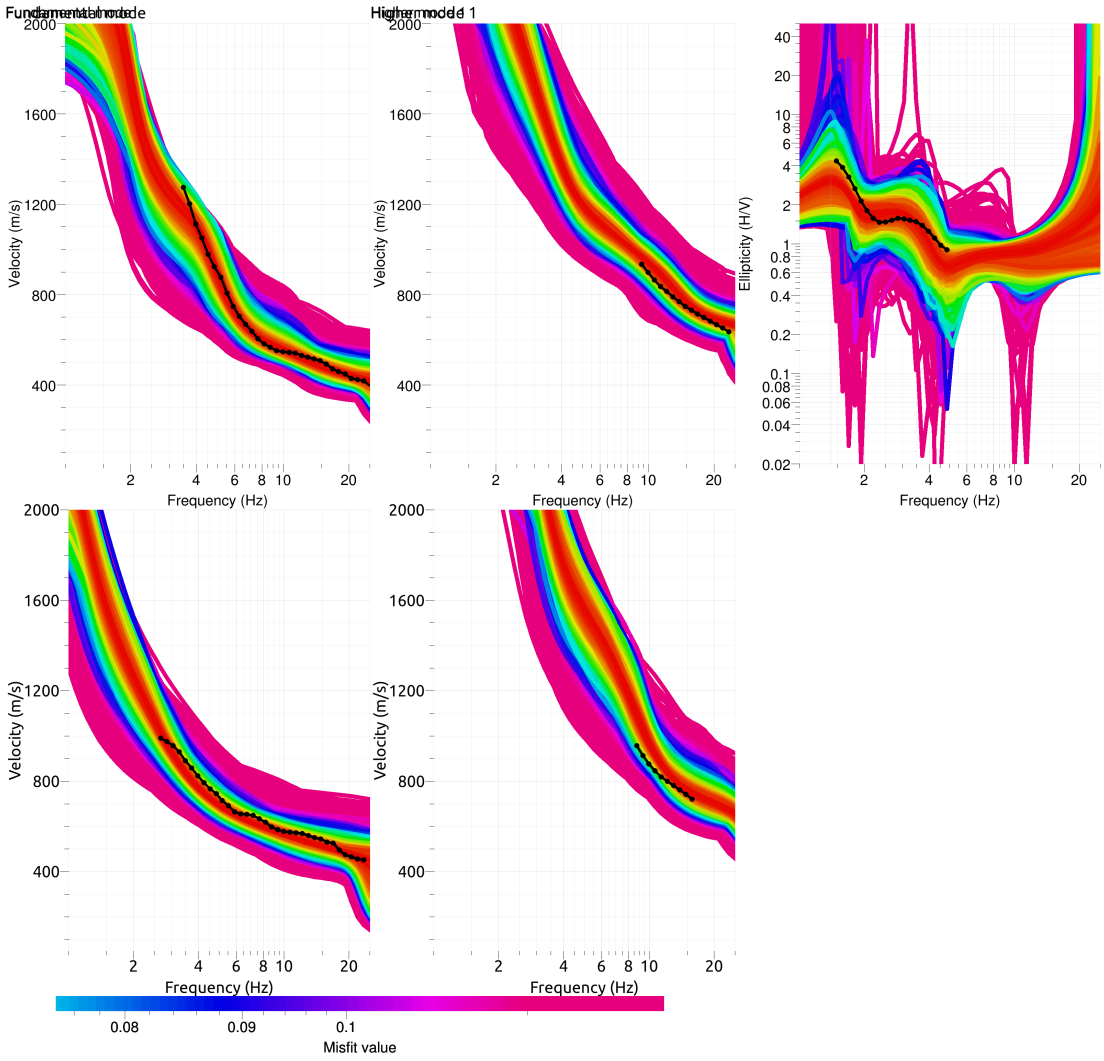

Figure 11: Comparison between inverted models and measured Rayleigh and Love modes and corresponding ellipticity, fixed layer depth strategy.

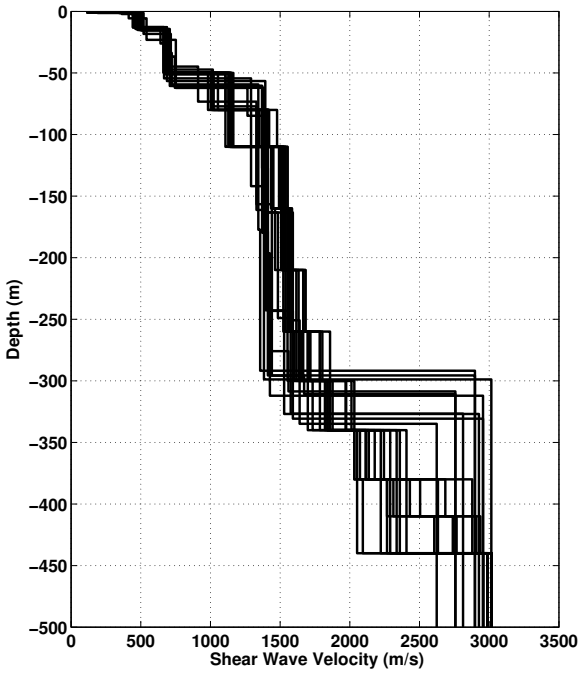

Figure 12: V_s ground profiles for the selected 25 best models.

6.2 Boreholes and interpretation

Assuming the slope of the mountain slopes aside the valley is constant below the sediments of the Rhone, the bedrock depth can also be estimated. The slope is around $40\,^\circ$ which corresponds to a depth of about $400\,\mathrm{m}$ at the station site, which is in accordance with what was found here. It can be noticed that the altitude of the bedrock is nearly 0 a.s.l..

Moreover, boreholes collected and provided by the Vaud canton on their geoportal (`http://www.geoplanet.vd.ch`) in the surroundings are giving more information about the nature of the underground (Fig. 13). Borehole number 3510, provided by the company Karakas & Français, is located in the array but is unfortunately only $8\,\mathrm{m}$ deep. The log shows $2\,\mathrm{m}$ of anthropogenic infill and $6\,\mathrm{m}$ of gravels. Some geotechnical tests were performed on these core samples. Borehole 6031 is located slightly further but goes down to $160\,\mathrm{m}$ without reaching the bedrock. The 4 first meters are made of infills, then, down to $20\,\mathrm{m}$, limestone is found (probably limestone gravels), the so called "Cône de la Grande Eau" or "Fan of the big water", meaning that water is flowing in this layer. Below this limit, alluvia of the Rhone with different quality are found.

We can therefore interpret the two first inverted layers, down to $45-60\,\mathrm{m}$, as various gravels of the "Cône de la Grande Eau". It can be noticed that the array is located in the central part of the alluvial fan, whereas borehole 6031 is located on the edge, explaining why its thickness is larger. As a comparison, borehole 6436 shows more than $90\,\mathrm{m}$ thickness of alluvial fan. Below the alluvial fan, the compacted alluvia of the Rhone are found down to the bedrock, at around $350\,\mathrm{m}$.

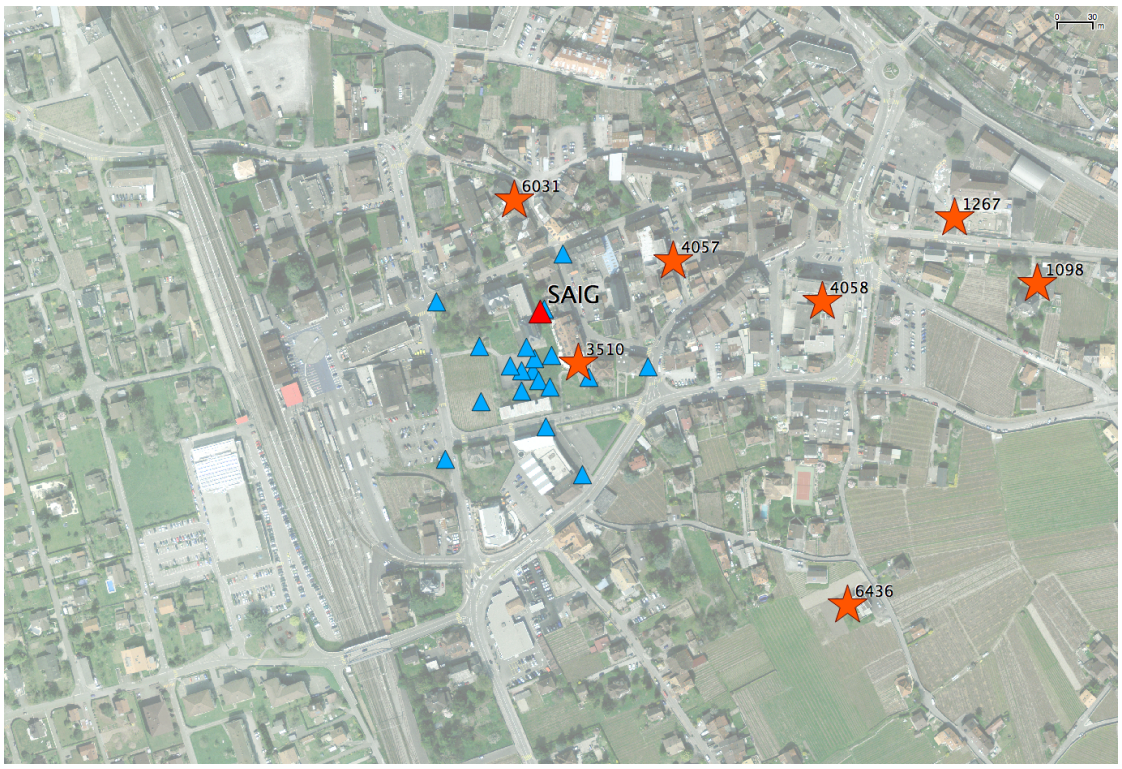

Figure 13: Available boreholes around the station SAIG.

6.3 Travel time average velocities and ground type

The distribution of the travel time average velocities at different depths was computed from the selected models. The uncertainty, computed as the standard deviation of the distribution of travel time average velocities for the considered models, is also provided, but its meaning is doubtful. $V_{s,30}$ is found to be $535\,\mathrm{m/s}$, meaning the site can be classified as class B in Eurocode 8 [CEN, 2004] and SIA261 [SIA, 2003].

6.4 SH transfer function and quarter-wavelength velocity

The quarter-wavelength velocity approach [Joyner et al., 1981] provides, for a given frequency, the average velocity at a depth corresponding to 1/4 of the wavelength of interest. It is useful to identify the frequency limits of the experimental data (minimum frequency in ellipticity $1.4\,\mathrm{Hz}$ and in dispersion curves, $2.7\,\mathrm{Hz}$). The results using this proxy show that the dispersion data are controlling the results down to $60\,\mathrm{m}$ and the ellipticity down to $189\,\mathrm{m}$ only (Fig. 14). Moreover, the quarter wavelength impedance-contrast introduced by Poggi et al. [2012] is also displayed in the figure. It corresponds to the ratio between two quarter-wavelength average velocities, respectively from the top and the bottom part of the velocity profile, at a given frequency [Poggi et al., 2012]. It shows a trough (inverse shows a peak) at the resonance frequency.
Moreover, the theoretical SH-wave transfer function for vertical propagation [Roesset, 1970] is computed from the inverted profiles. It is compared to the quarter-wavelength amplification [Joyner et al., 1981], that however cannot take resonances into account (Fig. 15). In this case, the

	Mean (m/s)	**Uncertainty (m/s)**
$V_{s,5}$	375	65
$V_{s,10}$	420	35
$V_{s,20}$	485	25
$V_{s,30}$	535	21
$V_{s,40}$	566	20
$V_{s,50}$	587	20
$V_{s,100}$	777	20
$V_{s,150}$	912	16
$V_{s,200}$	1009	14

Table 7: Travel time averages at different depths from the inverted models. Uncertainty is given as one standard deviation from the selected profiles.

models are predicting an amplification up to a factor of 4 at the frequency $3\,\mathrm{Hz}$, corresponding to the resonance of the "Cône de la Grande Eau" gravels. This will be compared to observations at this station.

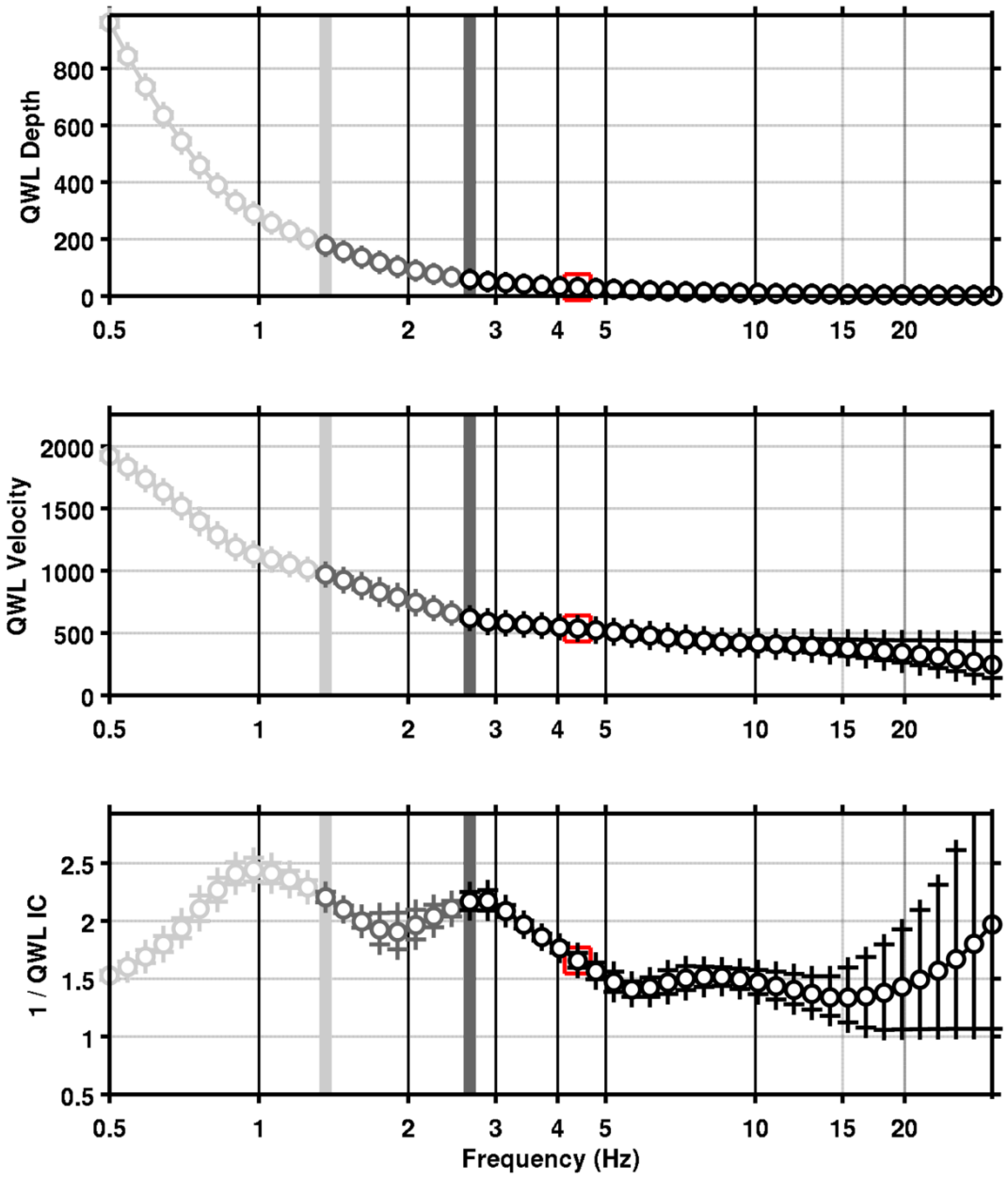

Figure 14: Quarter wavelength velocity representation of the velocity profile (top: depth, centre: velocity, bottom: inverse of the impedance contrast). Black curve is constrained by the dispersion curves, light grey is not constrained by the data. Red square is corresponding to $V_{s,30}$.

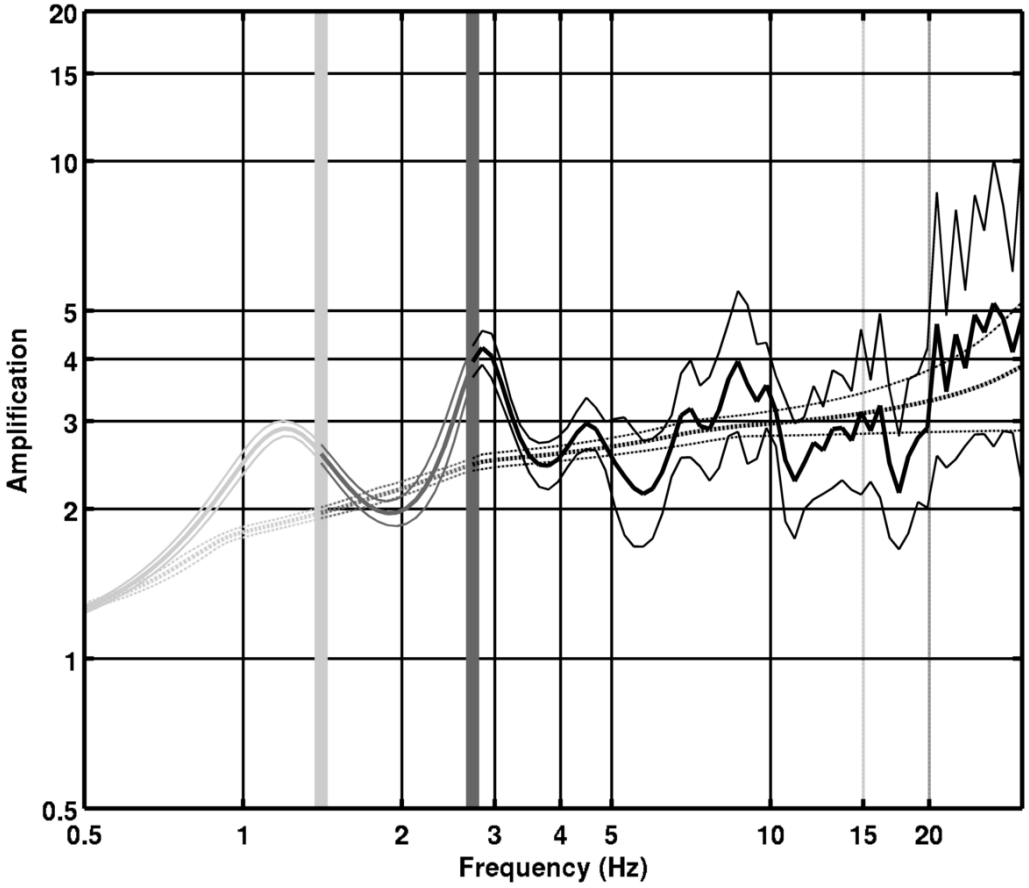

Figure 15: Theoretical SH transfer function (solid line) and quarter wavelength impedance contrast (dashed line) with their standard deviation. Significance of the greyshades is detailed in Fig. 14.

7 Conclusions

The array measurements presented in this study were successful in deriving a velocity model for the SAIG site in Aigle, close to the city centre. We found the alluvial fan of the "Cône de la Grande Eau", made of gravels, approximately on the first $50\,\mathrm{m}$. This alluvial fan is divided in 2 layers with an interface at about $15\,\mathrm{m}$ and velocities of 500 and $700\,\mathrm{m/s}$, respectively. Below, the consolidated sediments of the Rhone ($1500\,\mathrm{m/s}$) can be considered as rock. The bedrock is found at $350\,\mathrm{m}$ depth. The fundamental resonance frequency is $1.4\,\mathrm{Hz}$, with a peak amplitude around 4, with a polarized motion in the direction of the alluvial fan, therefore possibly corresponding to a 2D/3D behaviour of this structure. $V_{s,30}$ is found equal to $535\,\mathrm{m/s}$, corresponding to ground type B for EC8 and SIA261. The theoretical SH transfer function and impedance contrast of the quarter-wavelength velocity computed from the inverted profiles show an amplification up to 4 at $3\,\mathrm{Hz}$, corresponding to the resonance of the "Cône de la Grande Eau" gravels. Recordings of the new station will allow to validate these simple models.

Acknowledgements

The authors thank Mrs Roussy and Iufer that allowed these measurements, as well as the company Karakas & Français who provided borehole logs.

References

Sylvette Bonnefoy-Claudet, Fabrice Cotton, and Pierre-Yves Bard. The nature of noise wavefield and its applications for site effects studies. *Earth-Science Reviews*, 79(3-4): 205–227, December 2006. ISSN 00128252. doi: 10.1016/j.earscirev.2006.07.004. URL http://linkinghub.elsevier.com/retrieve/pii/S0012825206001012.

Jan Burjánek, Gabriela Gassner-Stamm, Valerio Poggi, Jeffrey R. Moore, and Donat Fäh. Ambient vibration analysis of an unstable mountain slope. *Geophysical Journal International*, 180(2):820–828, February 2010. ISSN 0956540X. doi: 10.1111/j.1365-246X.2009.04451.x. URL http://doi.wiley.com/10.1111/j.1365-246X.2009.04451.x.

J. Capon. High-Resolution Frequency-Wavenumber Spectrum Analysis. *Proceedings of the IEEE*, 57(8):1408–1418, 1969.

CEN. *Eurocode 8: Design of structures for earthquake resistance - Part 1: General rules, seismic actions and rules for buildings*. European Committee for Standardization, en 1998-1: edition, 2004.

Donat Fäh, Fortunat Kind, and Domenico Giardini. A theoretical investigation of average H / V ratios. *Geophysical Journal International*, 145:535–549, 2001.

Donat Fäh, Gabriela Stamm, and Hans-Balder Havenith. Analysis of three-component ambient vibration array measurements. *Geophysical Journal International*, 172(1):199–213, January 2008. ISSN 0956540X. doi: 10.1111/j.1365-246X.2007.03625.x. URL http://doi.wiley.com/10.1111/j.1365-246X.2007.03625.x.

Donat Fäh, Marc Wathelet, Miriam Kristekova, Hans-Balder Havenith, Brigitte Endrun, Gabriela Stamm, Valerio Poggi, Jan Burjanek, and Cécile Cornou. Using Ellipticity Information for Site Characterisation Using Ellipticity Information for Site Characterisation. Technical report, NERIES JRA4 Task B2, 2009.

William B. Joyner, Richard E. Warrick, and Thomas E. Fumal. The effect of Quaternary alluvium on strong ground motion in the Coyote Lake, California, earthquake of 1979. *Bulletin of the Seismological Society of America*, 71(4):1333–1349, 1981.

Katsuaki Konno and Tatsuo Ohmachi. Ground-Motion Characteristics Estimated from Spectral Ratio between Horizontal and Vertical Components of Microtremor. *Bulletin of the Seismological Society of America*, 88(1):228–241, 1998.

Valerio Poggi and Donat Fäh. Estimating Rayleigh wave particle motion from three-component array analysis of ambient vibrations. *Geophysical Journal International*, 180(1):251–267, January 2010. ISSN 0956540X. doi: 10.1111/j.1365-246X.2009.04402.x. URL http://doi.wiley.com/10.1111/j.1365-246X.2009.04402.x.

Valerio Poggi, Benjamin Edwards, and D. Fah. Characterizing the Vertical-to-Horizontal Ratio of Ground Motion at Soft-Sediment Sites. *Bulletin of the Seismological Society of America*, 102(6):2741–2756, December 2012. ISSN 0037-1106. doi: 10.1785/0120120039. URL http://www.bssaonline.org/cgi/doi/10.1785/0120120039.

J.M. Roesset. Fundamentals of soil amplification. In R. J. Hansen, editor, *Seismic Design for Nuclear Power Plants*, pages 183–244. M.I.T. Press, Cambridge, Mass., 1970. ISBN 978-0-262-08041-5. URL http://mitpress.mit.edu/catalog/item/default.asp?ttype=2\&tid=5998.

SIA. *SIA 261 Actions sur les structures porteuses*. Société suisse des ingénieurs et des architectes, Zürich, sia 261:20 edition, 2003.

Marc Wathelet. An improved neighborhood algorithm: Parameter conditions and dynamic scaling. *Geophysical Research Letters*, 35(9):1–5, May 2008. ISSN 0094-8276. doi: 10.1029/2008GL033256. URL http://www.agu.org/pubs/crossref/2008/2008GL033256.shtml.